Dependence of the vortex configuration on the geometry of mesoscopic flat samples

B. J. Baelus and F. M. Peeters*
Departement Natuurkunde, Universiteit Antwerpen (UIA), Universiteitsplein 1, B-2610 Antwerpen, Belgium
(Received 28 June 2001; revised manuscript received 7 December 2001; published 26 February 2002)

The influence of the geometry of a thin superconducting sample on the penetration of the magnetic field lines and the arrangement of vortices are investigated theoretically. We compare the vortex state of superconducting disks, squares, and triangles with the same surface area having nonzero thickness. The coupled nonlinear Ginzburg-Landau equations are solved self-consistently and the important demagnetization effects are taken into account. We calculate and compare quantities such as the free energy, the magnetization, the Cooper-pair density, the magnetic field distribution, and the superconducting current density for the three geometries. For given vorticity the vortex lattice is different for the three geometries, i.e., it tries to adapt to the geometry of the sample. This also influences the stability range of the different vortex states. For certain magnetic field ranges we found a coexistence of a giant vortex placed in the center and single vortices towards the corners of the sample. The *H-T* phase diagram is obtained for the three investigated geometries and we found that the critical magnetic field is substantially enhanced for the triangle geometry.

DOI: 10.1103/PhysRevB.65.104515 PACS number(s): 74.60.Ge, 74.20.De, 74.80.−g

I. INTRODUCTION

In mesoscopic samples there is competition between a triangle configuration of the vortex lattice, being the lowest-energy configuration in bulk material (and films), and the boundary, which tries to impose its geometry on the vortex lattice. For example, a circular geometry will favor vortices situated on a ring near the boundary, and only far away from the boundary its influence diminishes and the triangular lattice may reappear. Therefore, it is expected that different geometries will favor different arrangements of vortices and will make certain vortex configurations more stable than others. In small systems vortices may overlap so strongly that it is more favorable to form one big giant vortex. The latter will preferably have a circular geometry. As a consequence it is expected that the giant to multivortex transition will be strongly influenced by the geometry of the boundary as will also be the stability of the giant vortex configuration.

These issues and the dependence of the stability of the giant vortex configuration and of the different multivortex configurations on the geometry of the sample will be investigated in the present paper. As an example, we will compare the most important geometries: the circular disk, the square, and the triangle.

Mesoscopic (circular) disks and rings have been the most popular in this respect. Experimentally, the magnetization of superconducting disks and rings has been measured as a function of the externally applied magnetic field.[1–3] Several transitions between different superconducting states were found, and the magnetization depends sensitively on size and temperature. The main part of the theoretical studies covered disks[4–8] and rings[9–11] of zero thickness. In this case one can neglect the magnetic field induced by the supercurrents and one assumes that the total magnetic field equals the externally applied magnetic field, which is uniform. A limited number of studies considered disks[12–15] and rings[16] with *finite* thickness. Then, the finite thickness of the disks influences the magnetic field profile and it is necessary to take into account the demagnetization effects. Often only the (circular symmetric) giant vortex states or the superconducting/normal transition were investigated. Even in type-I superconductors multivortex states in disks[5–7,14] and rings[16,11] were predicted. It was found that if the disk or the ring is large enough, the giant vortex nucleates into a multivortex state in which the vortices are situated on a ring. In a ring geometry, we found that breaking the circular symmetry through a noncentral location of the hole favors the multivortex state.[16] This means that by changing the geometry, the giant vortex state transits into a multivortex state.

Mesoscopic superconductors with noncircular geometries have attracted less attention. Moshchalkov *et al.*[17] measured the superconducting/normal transition in superconducting lines, squares, and square rings using resistance measurements. Bruyndoncx *et al.*[18] calculated the *H-T* phase diagram for a square with zero thickness in the framework of the linearized Ginzburg-Landau theory, which is only valid near the superconducting/normal boundary. They compared their results with the *H-T* phase boundary obtained from resistance measurements. Fomin *et al.*[19] studied square loops with leads attached to it and found inhomogeneous Cooper-pair distributions in the loop with enhancements near the corners of the square loop. Schweigert and Peeters,[13,15] calculated the nucleation field as a function of the sample area for disks, squares, and triangles with zero thickness. Jadallah *et al.*[20] computed the superconducting/normal transition for mesoscopic disks and squares of zero thickness. For macroscopic squares, the magnetic field distribution and the flux penetration are investigated in detail by experimental observations using the magneto-optical Faraday effect and by first-principles calculations that describe the superconductor as a nonlinear anisotropic conductor.[21] In the latter case the penetration of the magnetic field occurs continuously. In macroscopic samples the penetration of individual fluxoids is not so important in the theoretical description of the magnetic response of the superconductor, but it turns out to be essential in our mesoscopic samples. Recently, Aftalion and Du[22] studied cylindrical square-shaped superconductors within the Ginzburg-Landau theory.

Chibotaru *et al.* investigated the vortex entry and the nucleation of antivortices in infinitely thin superconducting squares[23] and triangles[24] using the linearized Ginzburg-Landau theory. Within this linear theory they studied the superconducting/normal transition and they found near this transition the nucleation of multivortices, antivortices, and combination of these two instead of the expected surface superconductivity. They found that those antivortices appear in order for the vortex state to preserve the symmetry of the sample boundary. They also calculated the *H-T* phase diagram for the square and the triangle. Recently, Bonča and Kabanov[25] studied the $\kappa\rightarrow\infty$ limit and extended those results for thin superconducting squares, focusing the nonlinear Ginzburg-Landau theory. Within this nonlinear theory they showed that the vortex/antivortex configuration becomes rapidly unstable when moving away from the superconducting/normal transition.

In the present paper we consider superconductors of finite thickness and study the vortex configurations deep inside the superconducting state, i.e., far from the superconducting/normal boundary, for arbitrary value of κ. Our main focus will be on the influence of the geometry of the superconductor on the vortex configuration and its stability. Our theoretical analysis is based on a full self-consistent numerical solution of the coupled nonlinear Ginzburg-Landau (GL) equations for arbitrary value of κ. No *a priori* shape or arrangement of the vortex configuration is assumed. The magnetic field profile near and in the superconductor is obtained self-consistently, and therefore the full demagnetization effect is included in our approach.

The paper is organized as follows: In Sec. II we describe the theoretical formalism. Our results are presented in Sec. III. We calculate and compare the free energy and the magnetization for disks, squares, and triangles with the same surface area. Next, we make a distinction between multivortex states and giant vortex states and we investigate the influence of the sample geometry on the vortex lattice. We also calculate the magnetic field range over which the vortex states with vorticity L are stable in disks, squares, and triangles. The magnetic field distribution and the current density are studied and the *H-T* phase diagram is obtained. Finally, we summarize our results in Sec. IV.

II. THEORETICAL FORMALISM

In the present paper, we consider thin superconducting samples having the same volume but with different geometry which are immersed in an insulating medium in the presence of a perpendicular uniform magnetic field H_0. To solve this problem we follow the numerical approach of Schweigert and co-workers.[14] As for thin disks ($d\ll\xi,\lambda$) it is allowed to average the GL equations over the disk thickness for samples of arbitrary geometry. Using dimensionless variables and the London gauge $\mathrm{div}\vec{A}=0$ for the vector potential $\vec{A}$, we write the system of GL equations in the following form:

$$(-i\vec{\nabla}_{2D}-\vec{A})^2\Psi=\Psi(1-|\Psi|^2), \tag{1a}$$

$$-\Delta_{3D}\vec{A}=\frac{d}{\kappa^2}\delta(z)\vec{j}_{2D}, \tag{1b}$$

where

$$\vec{j}_{2D}=\frac{1}{2i}(\Psi^*\vec{\nabla}_{2D}\Psi-\Psi\vec{\nabla}_{2D}\Psi^*)-|\Psi|^2\vec{A}, \tag{1c}$$

is the density of superconducting current. The superconducting wave function satisfies the boundary conditions $(-i\vec{\nabla}_{2D}-\vec{A})\Psi|_n=0$ normal to the sample surface and $\vec{A}=\frac{1}{2}H_0\rho\vec{e}_\phi$ far away from the superconductor. Here the distance is measured in units of the coherence length ξ, the vector potential in $c\hbar/2e\xi$, and the magnetic field in $H_{c2}=c\hbar/2e\xi^2=\kappa\sqrt{2}H_c$. The superconductor is placed in the (x,y) plane, the external magnetic field is directed along the z axis, and the indices 2D, 3D refer to two- and three-dimensional operators, respectively.

To solve the system of Eqs. (1a) and (1b), we generalized the approach of Ref. 14 for circular disks to superconductors with an arbitrary flat geometry. We apply a finite-difference representation for the order parameter and the vector potential on a uniform Cartesian space grid (x,y), with typically 128×128 grid points for the area of the superconductor, and use the link variable approach[26] and an iteration procedure based on the Gauss-Seidel technique to find Ψ. The vector potential is obtained with the fast Fourier transform technique where we set $\vec{A}_{|x|=R_S,|y|=R_S}=H_0(x,-y)/2$ at the boundary of a box with a larger space grid of size typically 4 times the superconductor area.

For circular configurations such as disks the giant vortex state is characterized by the total angular momentum L through $\Psi=\psi(\rho)\exp(iL\phi)$, where ρ and ϕ are the cylindrical coordinates. L is the winding number and gives the vorticity of the system. Due to the nonlinearity of the GL equations an arbitrary superconducting state is generally a mixture of different angular harmonics L even in axially symmetric systems. Nevertheless, we can introduce an analog to the total angular momentum L, which is still a good quantum number and which is in fact nothing else then the number of vortices in the system.

For nonaxially symmetric systems there exist no axially symmetric giant vortex states, and hence the superconducting state is always a mixture of different angular harmonics. The vorticity L of a particular superconducting sample can be calculated by considering the phase φ of the order parameter along a closed loop near the boundary of the sample, where the total phase difference is always $\Delta\varphi=L\times2\pi$. In nonaxially symmetric systems three possible vortex states exist: (i) a multivortex state that contains separate vortices, (ii) a superconducting state that contains one giant vortex in the center, and (iii) a state that is a mixture of both: a giant vortex in the center surrounded by single vortices. The giant vortex is not necessarily circular symmetric as in the case of a circular disk, but it may be deformed due to the specific shape of the sample boundary.

To find the different vortex configurations, which include the metastable states, we search for the steady-state solutions

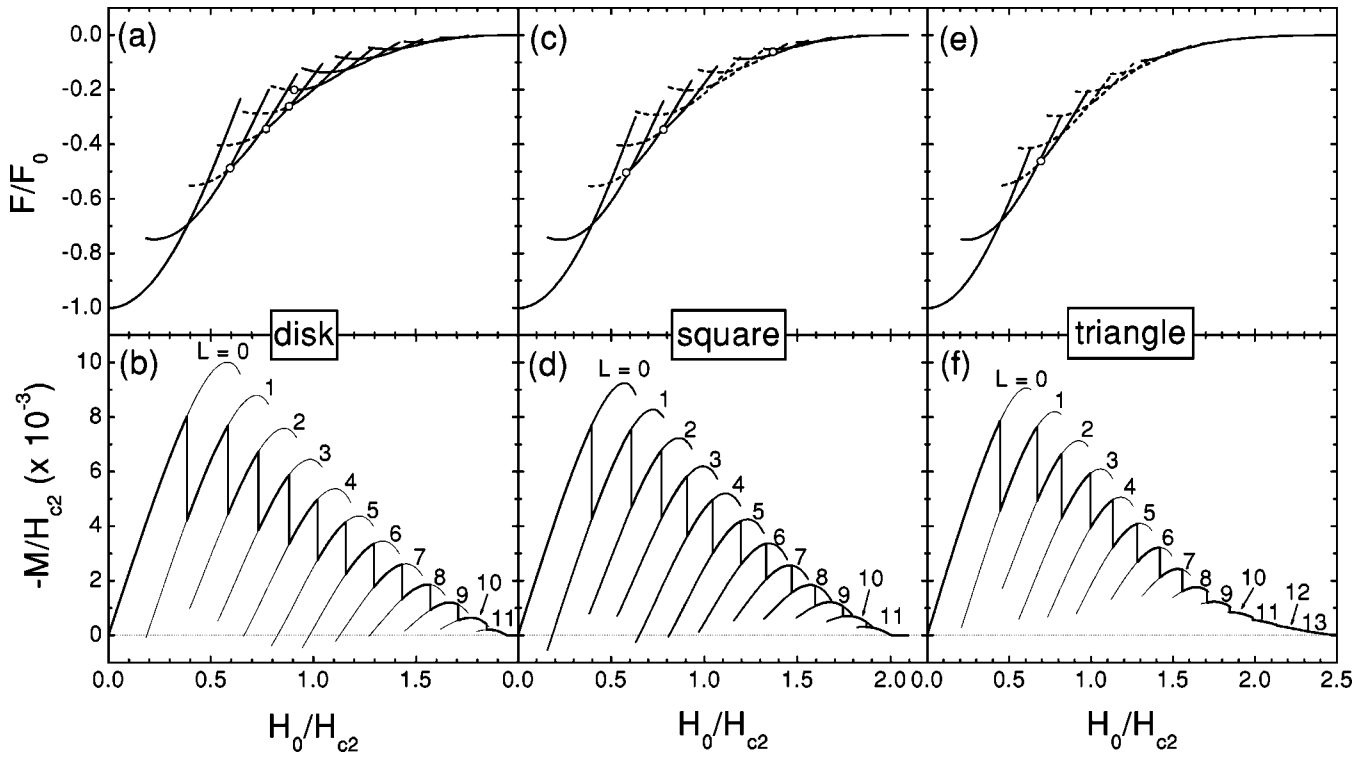

FIG. 1. The free energy and the magnetization as a function of the applied magnetic field for the disk, the square, and the triangle with the same surface area $S=\pi 16\xi^2$ and thickness $d=0.1\xi$ for $\kappa=0.28$. (a,c,e) The free energy of the giant vortex state (solid curves) and the multivortex states (dashed curves) and the multivortex to giant vortex transition fields (open circles). (b,d,f) The magnetization of the L states (solid curves) and the ground state (thick solid curve).

of Eqs. (1a) and (1b) starting from different randomly generated initial conditions. Then we increase/decrease slowly the magnetic field and recalculate each time the exact vortex structure. We do this for each vortex configuration in a magnetic field range where the number of vortices stays the same. By comparing the dimensionless Gibbs free energies of the different vortex configurations,

$$F=V^{-1}\int_V [2(\vec{A}-\vec{A}_0)\cdot\vec{j}_{2D}-|\Psi|^4]d\vec{r}, \tag{2}$$

where integration is performed over the sample volume V, and $\vec{A}_0$ is the vector potential of the uniform magnetic field, we find the ground state, the metastable states, and the magnetic field range over which the different states are stable. The dimensionless magnetization, which is a direct measure of the expelled magnetic field from the sample, is defined as

$$M=\frac{\langle H\rangle-H_0}{4\pi}, \tag{3}$$

where H_0 is the applied magnetic field. $\langle H\rangle$ is the magnetic field averaged over the sample and $\vec{H}=\mathrm{rot}\vec{A}$.

The temperature is indirectly included in ξ, λ, H_{c2}, whose temperature dependence is given by

$$\xi(T)=\frac{\xi(0)}{\sqrt{|1-T/T_{c0}|}}, \tag{4a}$$

$$\lambda(T)=\frac{\lambda(0)}{\sqrt{|1-T/T_{c0}|}}, \tag{4b}$$

$$H_{c2}(T)=H_{c2}(0)\left|1-\frac{T}{T_{c0}}\right|, \tag{4c}$$

where T_{c0} is the critical temperature at zero magnetic field. We will only explicitly insert temperature if we consider the H-T phase diagrams, while the other calculations are for a certain fixed temperature. Notice further that the Ginzburg-Landau parameter $\kappa=\lambda/\xi$ is independent of the temperature.

III. RESULTS

As a typical example, we consider superconducting disks, squares, and triangles with the same surface area $S=\pi 16\xi^2$, the same finite thickness $d=0.1\xi$ and the same Ginzburg-Landau parameter $\kappa=0.28$, which is typical for Al.[2] Thus the superconducting disk has a radius $R=4.0\xi$, the square has a width $W=7.090\xi$, and the triangle has a width $W=10.774\xi$.

A. Free energy and magnetization

In the first step, we will compare the free energy and the magnetization for the three geometries. In Figs. 1(a) and 1(b) the free energy and the magnetization are shown for the disk as a function of the applied magnetic field, in Figs. 1(c) and 1(d) for the square and in Figs. 1(e) and 1(f) for the triangle.

In Figs. 1(a),1(c), and 1(e) the free energy of the different giant vortex states is given by solid curves and the free energy of the multivortex states by dashed curves. The open circles indicate the transition from multivortex state to giant vortex state at the transition fields H_{MG}. This transition is of second order.[14] Figures 1(b), 1(d), and 1(f) show the magnetization of the different L states with thin curves and the ground state is indicated by the thick curve. There exist vortex states with vorticity up to $L=11$ for the disk and the square and up to 13 for the triangle. The superconducting state is destroyed at $H_{c3}/H_{c2}\approx 1.95$ for the disk, at $H_{c3}/H_{c2}\approx 2.0$ for the square, and $H_{c3}/H_{c2}\approx 2.5$ for the triangle. Thus for samples with sharp corners the superconducting/normal transition moves to higher field (for fixed surface area).[15] Multivortex states can nucleate in the disk for vorticity $L=2$, 3, 4, and 5 and in the square and the triangle for $L=2$, 3, 4, 5, and 6. Moreover, for the disk, with increasing field, the multivortex state always transits to a giant vortex state for fixed L, while for the square and the triangle some L states are multivortex states over the whole magnetic field range. For the triangle this is the case for the states with vorticity $L=3$, 4, 5, and 6, and for the square for the states with $L=4$ and 5. This indicates that breaking the axial symmetry favors the multivortex state over the giant vortex state. In some magnetic field regions, the vortex states exhibit a paramagnetic response, i.e., $-M<0$. This occurs in the disk for metastable states with $L=1$, 4–8 and in the square for metastable states with $L=1$, 4, and 5. For the triangle $-M$ is always positive, i.e., only diamagnetic behavior is observed.

In order to stress the difference between macroscopic and our mesoscopic superconductors we show in Fig. 2(a) the magnetic flux $\phi_{L\to L+1}$ passing through the superconductor at the thermodynamic transition field $H_{L\to L+1}$ as a function of the vorticity L for the three geometries. We scaled this flux by $(L+1)\phi_0$, which is the expected flux when no boundary effects are important. The result for the disk is given by circles, for the square by squares and for the triangle by triangles. In the figure we use open symbols for transitions between two giant vortex states, filled symbols for transitions between a multivortex and a giant vortex state, and crossed symbols for transitions between two multivortex states. The symbol for the largest L corresponds to the superconducting/normal transition. For the disk we find $L\to L+1$ transitions between a giant vortex and a multivortex state for $L=1$ and 2, while the other transitions occur between two giant vortex states. For the square we find transitions between a multivortex state and a giant vortex state for $L=2$, 3, and 6 and between two multivortex states for $L=4$ and 5. For the triangle, transitions between a giant and a multivortex state occur for $L=1$, 2, and 6 and between two multivortex states for $L=2$, 3, and 4. Notice further that for $L>6$, the value of $\phi_{L\to L+1}/(L+1)\phi_0$ becomes almost independent of L for the three geometries: $\phi_{L\to L+1}/(L+1)\phi_0\approx 1.3$ for the disk and the square and $\phi_{L\to L+1}/(L+1)\phi_0\approx 1.4$ for the triangle. The magnetic flux $\phi_{L\to L+1}$ passing through the superconductor at the thermodynamic transition field $H_{L\to L+1}$ can be fitted by the following formula:

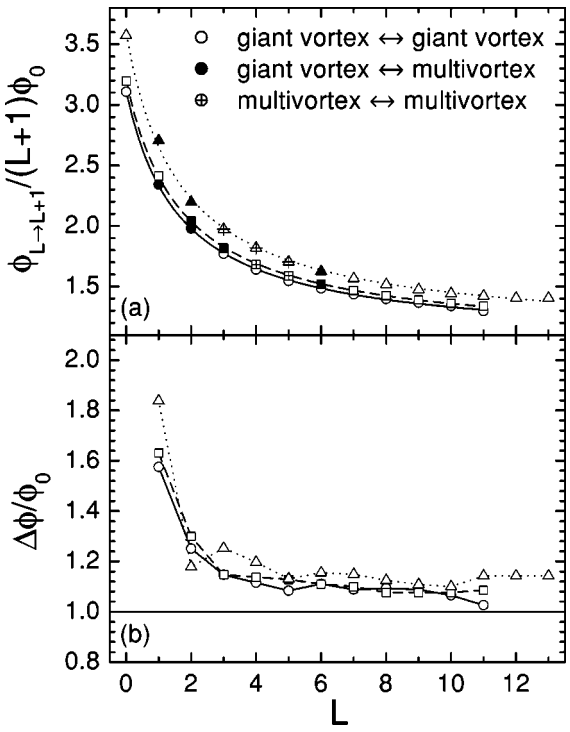

FIG. 2. (a) The flux $\phi_{L\to L+1}$ corresponding to the thermodynamic transition field $H_{L\to L+1}$ as a function of the vorticity L for the disk (circles), for the square (squares), and for the triangle (triangles). The curves are the fitted results. (b) The flux $\Delta\phi$ corresponding to the magnetic field range needed to increase the vorticity of the ground state from L to $L+1$ as a function of the vorticity L for the disk (solid curves, open circles), the square (dashed curve, open squares), and the triangle (dotted curve, open triangles).

$$\frac{\phi_{L\to L+1}}{(L+1)\phi_0}=\frac{a+bL}{1+cL},$$

with $a=3.108\,37$, $b=0.617\,92$, and $c=0.598\,25$ for the disk [solid curve in Fig. 2(a)], $a=3.197\,69$, $b=0.609\,62$, and $c=0.583\,96$ for the square (dashed curve), and $a=3.586\,14$, $b=0.661\,14$, and $c=0.6031$ for the triangle (dotted curve).

Another important quantity is the amount of flux increase needed to increase the vorticity of the ground state from L to $L+1$, which is plotted in Fig. 2(b) for the disk (solid curves, open circles), the square (dashed curve, open squares), and the triangle (dotted curve, open triangles). For $3<L<11$, this value is almost independent of L and of the geometry and equals $\Delta\phi/\phi_0\simeq 1.1$, i.e., it is approximately equal to, but still different from, the flux quantum ϕ_0. Notice that $\Delta\phi/\phi_0>1$ for any L, which is a consequence of the demagnetization effects.

B. Multivortex states

To distinguish whether the superconducting state is a multivortex state or a giant vortex state and to determine the multivortex to giant vortex state transition field, we considered the Cooper-pair density $|\Psi|^2_{\text{center}}$ in the center of the superconductor.[14] We can be sure that the superconducting state is a multivortex state if $|\Psi|^2_{\text{center}}\neq 0$ for $L>1$. The rea-

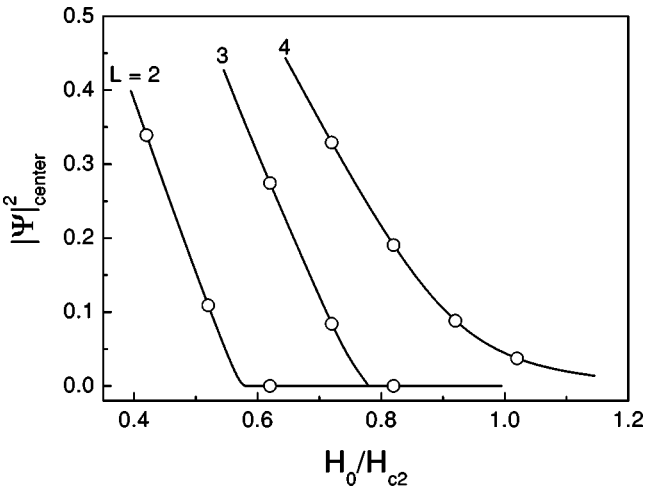

FIG. 3. The Cooper-pair density in the center of the square as a function of the applied magnetic field for the states with vorticity $L=2$, 3, and 4.

son is that giant vortices are always in the center of the superconductor, and hence $|\Psi|^2_{\text{center}}=0$. Figure 3 shows the Cooper-pair density in the center of the square as a function of the applied magnetic field. The Cooper-pair density $|\Psi|^2_{\text{center}}$ is finite for $H_0/H_{c2}<H_{GM}/H_{c2}\approx 0.5825$ and 0.7825 for $L=2$ and 3, respectively, and $|\Psi|^2_{\text{center}}=0$ for $H_0/H_{c2}>H_{GM}/H_{c2}$. For $L=4$ the Cooper-pair density in the center differs from zero over the whole magnetic field region where the $L=4$ state is stable. On the other hand, $|\Psi|^2_{\text{center}}=0$ does not guarantee that the superconducting state is a giant vortex state. For example, the multivortex state in a square for $L=5$ shows four vortices away from the center situated on the diagonals and one vortex in the center, and hence $|\Psi|^2_{\text{center}}=0$. Therefore, we studied the Cooper-pair density distribution in detail. If two vortices are very close to each other, then the Cooper-pair density on the axis between these two vortices will become very low too, which means that the separation between two vortices becomes invisible in the contour plots. Therefore we have to define another criterion to determine the multivortex to giant vortex transition. If the maximum between two minima in the Cooper-pair density (i.e., the vortices) is lower than 0.5% of the maximum Cooper-pair density $|\Psi|^2_{\text{max}}$ in the sample, then we will say that the vortices form a giant vortex state instead of a multivortex state. With this criterion we find that for the square geometry the $L=5$ state is always a multivortex state and the $L=6$ state is a multivortex state for $H_0/H_{c2}<1.37$ and a giant vortex state for $H_0/H_{c2}>1.37$.

How do the multivortex states look like? Figures 4(a)–4(c) show the Cooper-pair density for a multivortex state with $L=2$, 3, and 4 at $H_0/H_{c2}=0.42$, 0.67, and 0.745, respectively. High Cooper-pair density is given by dark regions and low Cooper-pair density by light regions. For $L=2$ the vortices are along the diagonal, for $L=3$ the vortices are on a triangle, and for $L=4$ they are on a square. For $L=4$ only the multivortex state is found, which is favored over the giant vortex state. The reason is that the square vortex lattice easily fits in the sample. Figures 4(d) and 4(e) show the

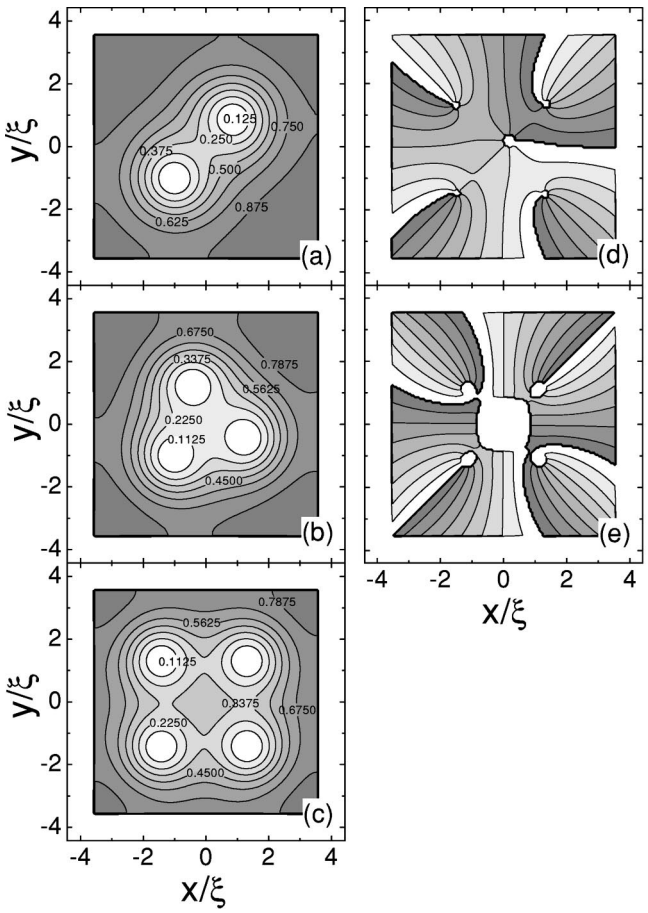

FIG. 4. (a–c) The Cooper-pair density for a multivortex state in a square with $L=2$, 3, and 4 at $H_0/H_{c2}=0.42$, 0.67, and 0.745, respectively. High Cooper-pair density is given by dark regions, low Cooper-pair density by light regions. (d,e) The phase of the order parameter for the multivortex states with $L=5$ at $H_0/H_{c2}=0.82$ and with $L=6$ at $H_0/H_{c2}=1.32$. Phases near zero are given by light regions and phases near 2π by dark regions.

phase of the order parameter for the multivortex states with $L=5$ at $H_0/H_{c2}=0.82$ and with $L=6$ at $H_0/H_{c2}=1.32$. Phases near zero are given by light regions and phases near 2π by dark regions. By going around the superconductor, the phase clearly changes $5\times 2\pi$ in Fig. 4(d) and $6\times 2\pi$ in Fig. 4(e). For $L=5$ there are four vortices on a square and the fifth vortex is in the center. The latter has clearly a vorticity of 1. For $L=6$ there are also four vortices on a square and the other vortices are in the center forming one giant vortex with a vorticity of 2. Thus in this case we have the remarkable coexistence of a giant vortex in the center with a vorticity of 2 and four clearly separated vortices around it. For this case the multivortex to giant vortex transition field is defined as the field where separate vortices appear with decreasing field. This means that in Fig. 1 some states are indicated as multivortex, even though there exists a (giant) vortex in the center with vorticity $L>1$. Thus we consider a state no longer a giant vortex state when the fluxes of the vortex are not confined in a single connected region. Notice also that not only the configuration of the multivortices tries

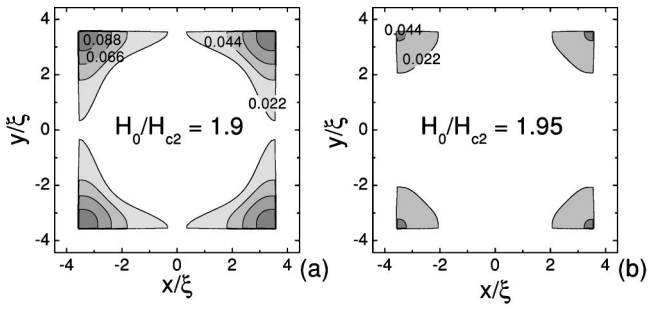

FIG. 5. The Cooper-pair density for the $L=11$ state in a square at $H_0/H_{c2}\approx 1.9$ (a) and 1.95 (b).

to have the same geometry as the sample, but also the giant vortex geometry depends on the sample geometry.

We found that for this size of the square sample, the states with $L>6$ are always in the giant vortex state. With increasing L this giant vortex grows and superconductivity only occurs in the corners of the square. This is illustrated in Figs. 5(a) and 5(b), which shows the Cooper-pair density for the $L=11$ state at $H_0/H_{c2}\approx 1.9$ and 1.95. It is obvious that further increasing the field pushes the superconducting condensate more to the corners. At the superconducting/normal transition field $H_0/H_{c2}\approx 2.0$ the corners become normal too. Only extremely close to the superconductor/normal transition the order parameter exhibits additional separate zeros in the central part of the sample that correspond to the predicted vortex/antivortex configurations. We refer to Refs. 23 and 24 for a detailed study of these states. But note that our calculation also provides the amplitude of the order parameter, which turns out to be very small ($|\Psi|<10^{-3}$) in the central area of the sample. As a consequence, additional zeros of the order parameter in this central region will lead to an extremely small variation of the Cooper-pair density ($|\Psi|^2<10^{-6}$). The corresponding variation in the magnetic field will also be extremely small ($\Delta H/H_0<10^{-5}$) and probably impossible to detect experimentally.

Figure 6 shows the positions of the vortices for the $L=3$ state in a square at applied magnetic fields $H_0/H_{c2}=0.545$, 0.62, 0.695, and 0.77. The latter field is just below the multivortex to giant vortex state transition field $H_{GM}/H_{c2}\approx 0.7825$. The solid lines indicate the square boundaries. With increasing field the vortices move towards the center of the square and at $H_{GM}/H_{c2}\approx 0.7825$ they combine in the center and form one giant vortex with vorticity $L=3$. In the multivortex state, one vortex is always situated on the diagonal of the square, regardless of the magnetic field. The other two vortices are located such that the three vortices form a equilateral triangle that is centered in the center of the square. Since the vortices move to the center with increasing field, the width W of the triangular vortex lattice decreases, i.e., $W=3.27$, 2.89, 2.32, and 1.61 at $H_0/H_{c2}=0.545$, 0.62, 0.695, and 0.77, respectively.

For the triangle geometry multivortex states nucleate with vorticity $L=2$, 3, 4, 5, and 6 [see Figs. 1(e) and 1(f)]. Figures 7(a)–7(c) show the Cooper-pair density for a multivortex state with $L=2$, 3, and 4 at $H_0/H_{c2}=0.495$, 0.82, and 0.745, respectively. High Cooper-pair density is given by

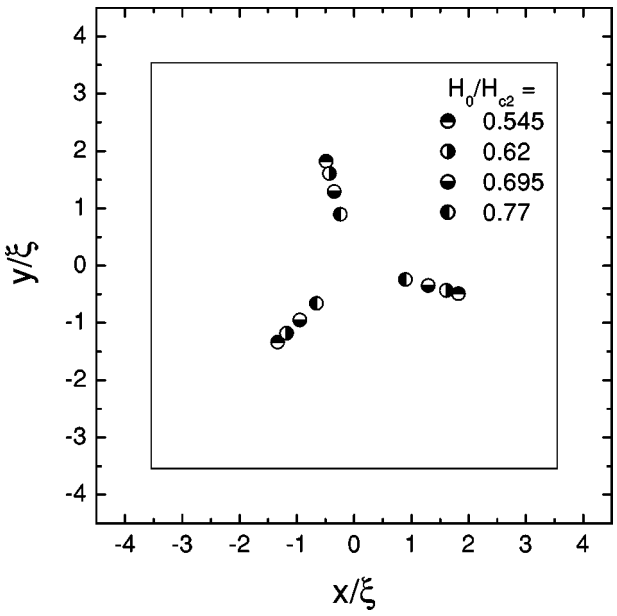

FIG. 6. The multivortex positions of the $L=3$ state in a square at applied magnetic fields $H_0/H_{c2}=0.545$, 0.62, 0.695, and 0.77.

dark regions and low Cooper-pair density by light regions. In the multivortex state with vorticity $L=2$ the vortices are situated along one of the perpendicular bisectors of the triangle. In the $L=3$ state the vortices are on a triangle that easily fits in the sample, while the $L=4$ state consists of three vortices on a triangle and the fourth vortex is situated in the center. Instead of the square configuration as in the case of the square geometry, the vortex lattice tries to copy the geometry of the sample, i.e., the triangular geometry. For the multivortex states with $L=5$ and $L=6$, the separation of vortices becomes invisible in the contour plots of the Cooper-pair density, which show one big vortex in the center. The reason is that the maximum Cooper-pair density on the axis between two vortices is very low. Therefore, we show the phase of the order parameter in Figs. 7(d) and 7(e) for the multivortex states with $L=5$ at $H_0/H_{c2}=1.27$ and with $L=6$ at $H_0/H_{c2}=1.345$. Phases near zero are given by light regions and phases near 2π by dark regions. In both cases there is a coexistence of a giant vortex in the center and three separated vortices around it placed in the direction of the corners. Taking a loop around the giant vortex, the phase changes, respectively, by $2\times 2\pi$ and $3\times 2\pi$, which means that the vorticity of the giant vortex is 2 in the case of the $L=5$ multivortex state and 3 in the case of the $L=6$ multivortex state. Notice also that for $L=6$ the geometry of the giant vortex is not axial symmetrical, but triangular. States with $L>6$ are always giant vortex states as we also found for the square. With increasing L this giant vortex grows, and for large vorticities superconductivity only occurs in the corners of the triangle. Further increasing the field pushes the superconductivity more to the corner until these corners become normal too at the superconducting/normal transition field.

For the circular disk we find multivortex states with vorticity $L=2$, 3, 4, and 5 [see Figs. 1(a) and 1(b)]. Figures. 8(a)–8(d) show the Cooper-pair density for the multivortex states with vorticity $L=2$, 3, 4, and 5 at $H_0/H_{c2}=0.495$,

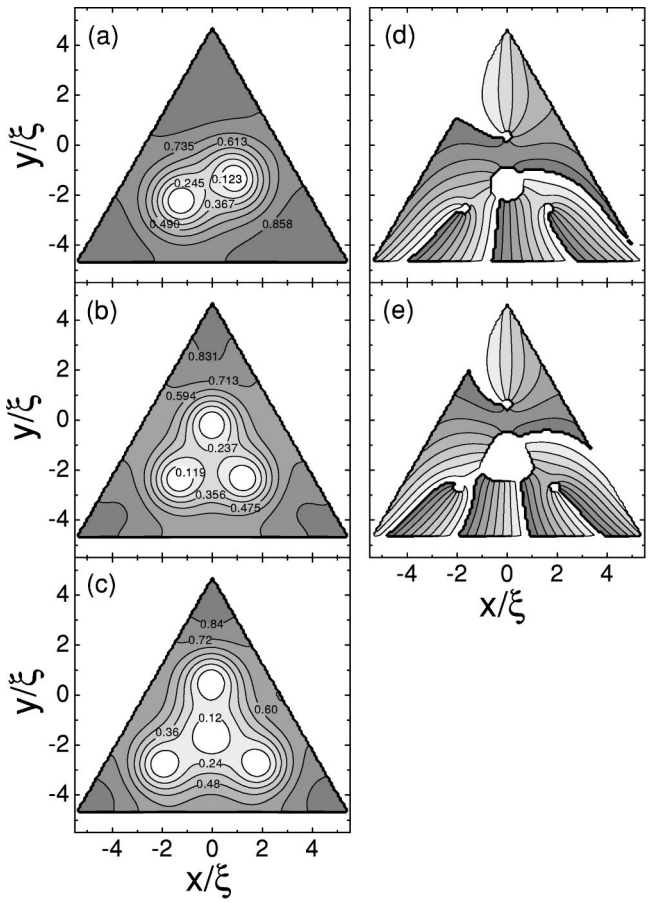

FIG. 7. (a–c) The Cooper-pair density for the multivortex states in a triangle with $L=2$, 3, and 4 at $H_0/H_{c2}=0.495$, 0.82, and 0.745, respectively. High Cooper-pair density is given by dark regions and low Cooper-pair density by light regions. (d,e) The phase of the order parameter for the multivortex states with $L=5$ at $H_0/H_{c2}=1.27$ and with $L=6$ at $H_0/H_{c2}=1.345$. Phases near zero are given by light regions, phase near 2π by dark regions.

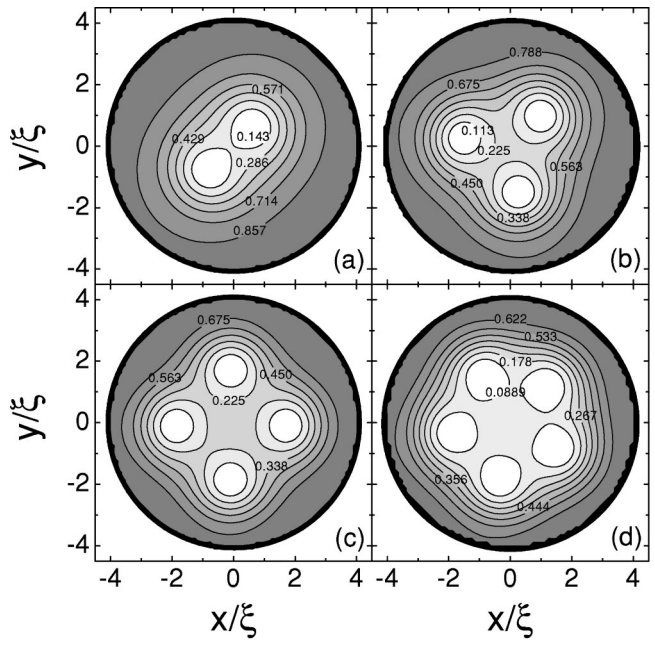

FIG. 8. (a–d) The Cooper-pair density for the multivortex states in a disk with vorticity $L=2$, 3, 4, and 5 at $H_0/H_{c2}=0.495$, 0.62, 0.965, and 0.82, respectively. High Cooper-pair density is given by dark regions and low by light regions.

0.62, 0.965, and 0.82, respectively. High Cooper-pair density is given by dark regions and low by light regions. Multivortex states for disks were already studied in previous papers (see the Introduction). Therefore, in this paper we only stress that in a disk the multivortices are positioned on a ring, which means that also in this case the sample imposes its symmetry on the vortex lattice.

From the study of the Cooper-pair density and the phase of the order parameter we learned that (i) multivortex states nucleate in disks as well as in squares and triangles for several values of the vorticity L, and (ii) the vortex lattices try to have the same geometry as the sample.

C. Magnetic field distributions: Demagnetization effects

Since we studied samples with finite thicknesses, demagnetization effects are important and therefore we had to solve for the magnetic field distribution around the sample. In this section we will describe the magnetic field distribution for the square. The results for the disk and the triangle are analogous.

In Figs. 9(a)–9(f) the magnetic field distribution is shown for the square geometry for the state with vorticity $L=2$ at $H_0/H_{c2}=0.42$, 0.52, and 0.62 (see open circles in Fig. 3), and with vorticity $L=3$ at $H_0/H_{c2}=0.62$, 0.72, and 0.82, respectively. High magnetic field is given by dark regions and low by light regions. The magnetic field is clearly nonuniform in and around the sample. The dark spots in the square are the vortices and the dark regions near the sample surface are due to the compression of the magnetic lines when they are forced to go around the sample. These regions are responsible for the demagnetization effects. It is clear that with increasing external field and fixed number of vortices, the demagnetization effects are more pronounced, because the superconductor has to expel more magnetic field. In Figs. 9(a), 9(b), 9(d), and 9(e) the superconducting state is a multivortex state and the separated vortices are clearly visible, while in Figs. 9(c) and 9(f) where $H_0/H_{c2} > H_{MG}/H_{c2} \approx 0.5825$ and 0.7825 for $L=2$ and 3, respectively, there is one giant vortex in the center. With increasing field the vortices move towards the center and at $H_0=H_{MG}$ they combine to one giant vortex state. Notice that the giant vortex state is not necessarily axial symmetric as in the case of the disk.

In Figs. 10(a)–10(d) the magnetic field distribution is shown for the square geometry for the state with vorticity $L=4$ at the magnetic fields indicated by the open circles in Fig. 3, i.e., $H_0/H_{c2}=0.72$, 0.82, 0.92, and 1.02, respectively. Now, there is no transition from the multivortex to giant vortex state and the four vortices are clearly visible as the dark spots. Notice that from the magnetic field distribution one clearly observes that the vortex lattice is a square lattice,

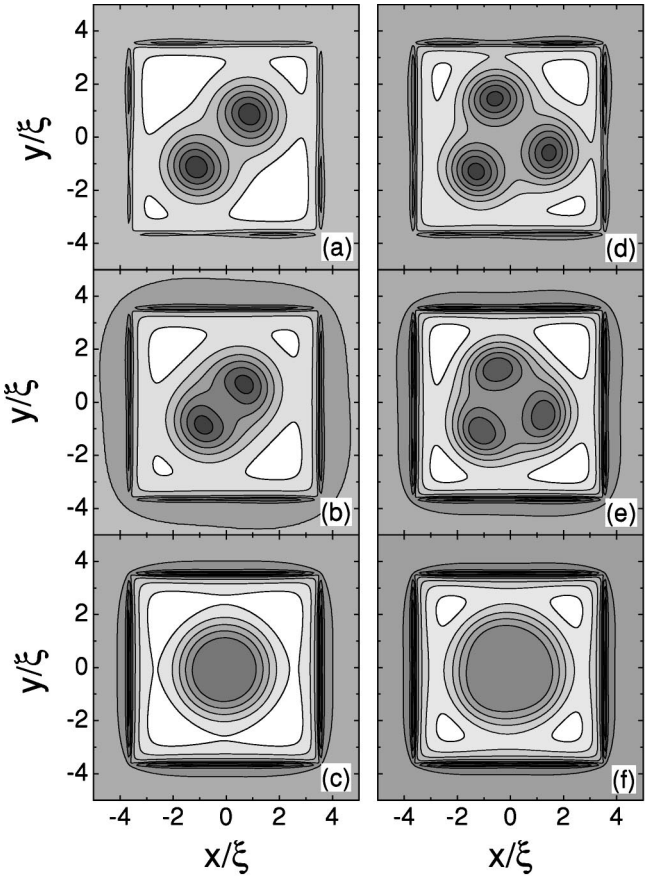

FIG. 9. The magnetic field distribution for the square for the state with vorticity $L=2$ at $H_0/H_{c2}=0.42$ (a), 0.52 (b), and 0.62 (c), and with vorticity $L=3$ at $H_0/H_{c2}=0.62$ (d), 0.72 (e), and 0.82 (f). High magnetic field is given by dark regions and low by light regions.

i.e., the lattice geometry is the same as the sample geometry, and that the vortices move towards the center with increasing field.

For the multivortex states with higher vorticity, the separated multivortices are no longer visible in the contour plots of the magnetic field distribution. The problem is the same as for the contour plots of the Cooper-pair density, i.e., the vortices are too close to each other and the spots corresponding to high magnetic fields are overlapping in the picture. For high vorticity and high external fields, the total magnetic field appreciably differs from the externally applied field only in the corners of the square. Figures 11(a) and 11(b) show the magnetic field distribution for the same configuration as in Figs. 5(a) and 5(b), i.e., the $L=11$ state at $H_0/H_{c2}\approx 1.9$ and 1.95, respectively. A local decrease in magnetic field is given by the light regions and an increase by the dark regions. In both pictures the magnetic field is only substantially expelled in the corners and consequently only near the corners is there a higher density of magnetic field lines at the outside of the square. Further increasing the field destroys the superconductivity, and thus the total field becomes equal to the external one over the whole sample.

Next, we investigate the dependence of the magnetic field on z. Figures 12(a)–12(f) show the magnetic field distribution for the $L=4$ state in a square for different values of z, $z/\xi=0.0$, 0.1, 0.3, 0.6, 1.0 and 10.0, respectively. The applied magnetic field is $H_0/H_{c2}=0.77$. High magnetic field is given by dark regions and low magnetic field by light regions. In the plane of the superconductor, i.e., $z=0$, the magnetic field that penetrates the superconductor is either compressed into multivortices or expelled to the outside of the sample. Therefore, the four dark spots in Fig. 12(a) indicate that the vortices and the light regions towards the sample boundary are due to the expulsion of the magnetic field towards the outside of the superconductor. As a consequence, the magnetic field increases in a small strip near the sample boundary. With increasing z and $|z|>d/2$, the magnetic field will still be influenced by the superconductor. The demagnetization effects decrease with increasing z and the compression of the magnetic field lines into vortices becomes smaller. Therefore, the vortices and the expulsion of the field

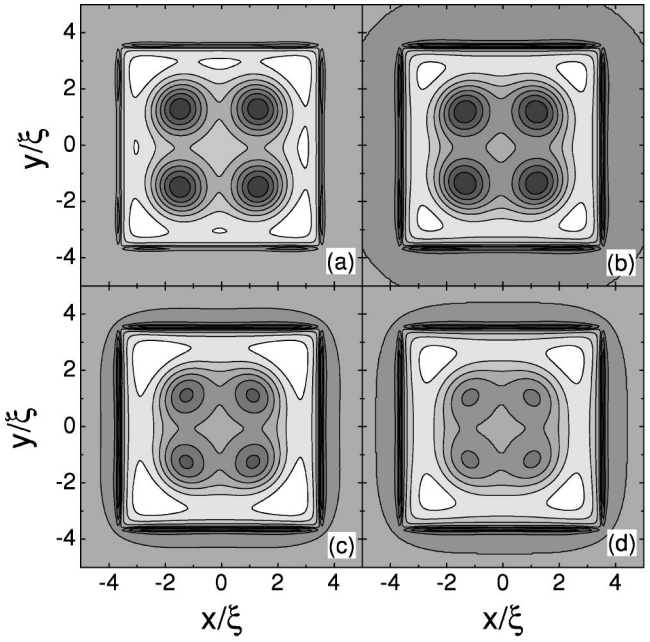

FIG. 10. The magnetic field distribution for the square for the state with vorticity $L=4$ at $H_0/H_{c2}=0.72$ (a), 0.82 (b), 0.92 (c), and 1.02 (d). High (low) magnetic fields are given by dark (light) regions.

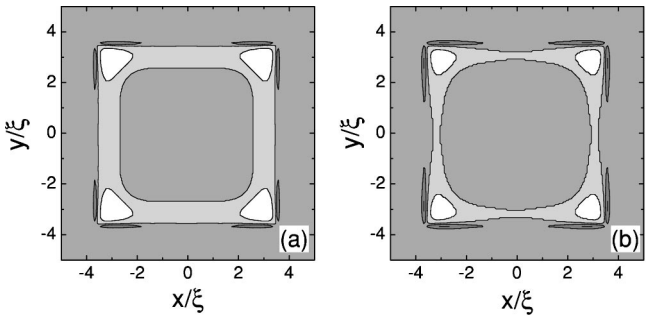

FIG. 11. The magnetic field distribution for the $L=11$ state in a square at $H_0/H_{c2}\approx 1.9$ (a) and 1.95 (b). High (low) magnetic fields are given by dark (light) regions.

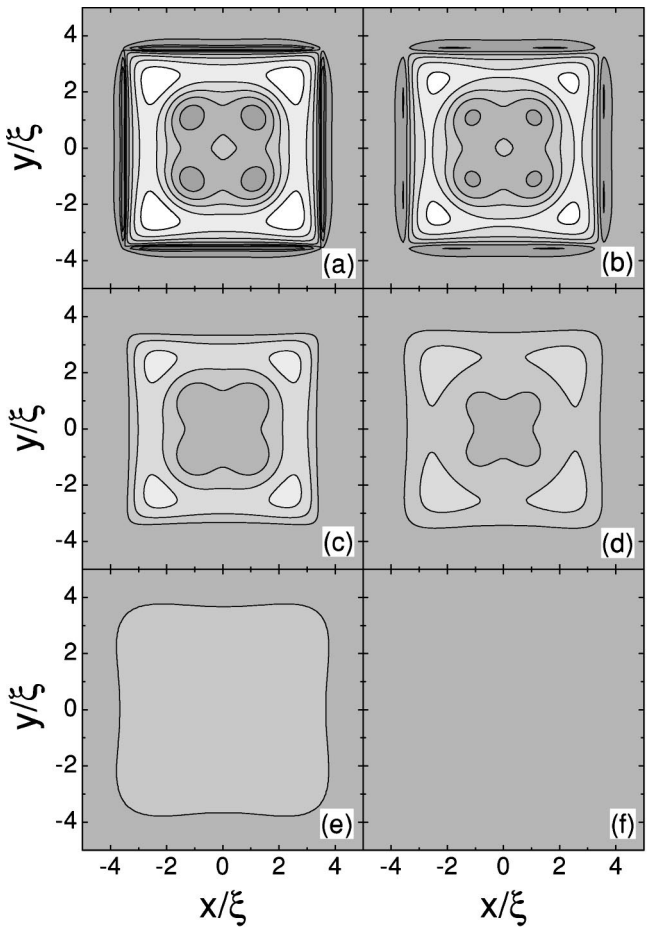

FIG. 12. The magnetic field distribution for the $L=4$ state in a square for different values of z; $z/\xi=0.0$ (a), 0.1 (b), 0.3 (c), 0.6 (d), 1.0 (e), and 10.0 (f). The applied magnetic field is $H_0/H_{c2}=0.77$. High magnetic field is given by dark regions, low magnetic field by light regions.

will become less pronounced with increasing z. At $z=0.1\xi$, the vortices and the results of the magnetic field expulsion are still visible by the dark and light regions [see Fig. 12(b)]. In Figs. 12(c) and 12(d), at $z=0.3\xi$ and 0.6ξ, respectively, the contrast in the picture decreases, which means that the influence of the superconductor, i.e., the compression and expulsion of the magnetic field lines, decreases. At $z=1.0\xi$ the magnetic field just slightly decreases right above the superconductor compared to the external field [see Fig. 12(e)]. At $z=10.0\xi$ the total magnetic field is homogeneous. Far away from the superconductor, the magnetic field is not influenced by the superconductor and equals the external field. This is clearly shown in Fig. 12(f).

D. Superconducting current density

When a superconducting sample is placed in an external magnetic field, the magnetic field is expelled from the superconductor due to screening currents near the sample boundary. The direction of the screening currents is such that the corresponding magnetic field is opposite to the external one, which leads to a lower total field in the superconductor. The magnetic field penetrating the superconductor creates currents flowing in a direction opposite to the screening currents. The competition between these currents and the screening currents results in the existence of vortices.

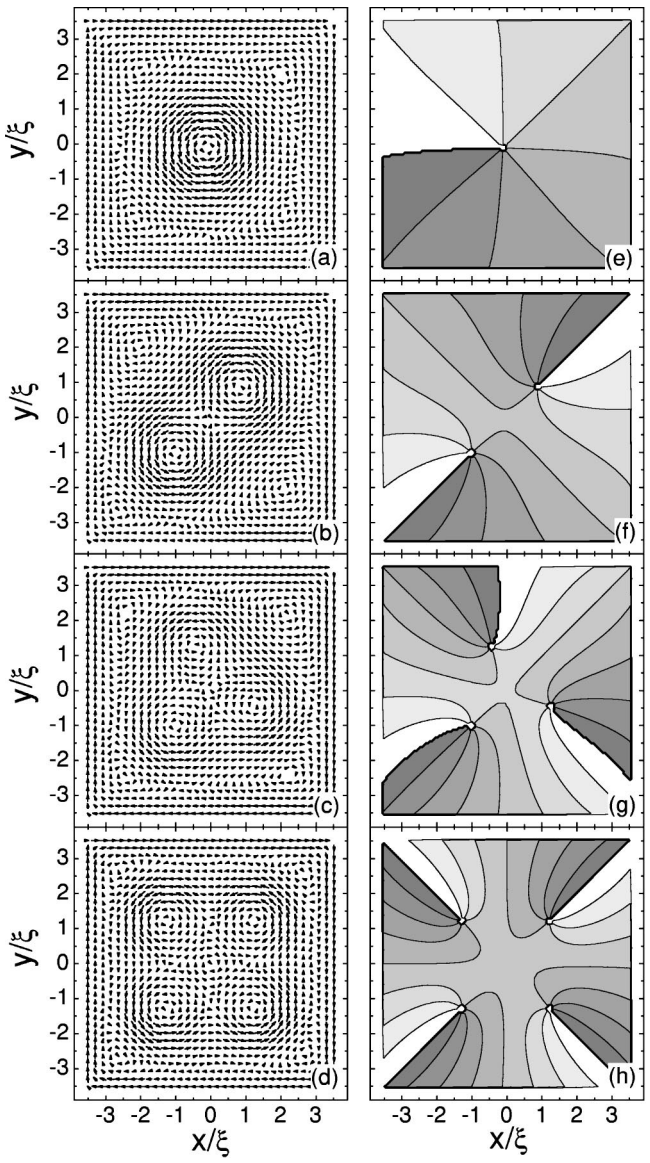

FIG. 13. (a–d) Vector plots of the supercurrent in the superconducting square and (e–h) contour plots of the phase of the order parameter for the $L=1$ state at $H_0/H_{c2}=0.27$ (a,e), the $L=2$ state at $H_0/H_{c2}=0.42$ (b,f), the $L=3$ state at $H_0/H_{c2}=0.67$ (c,g), and the $L=4$ state at $H_0/H_{c2}=0.745$ (d,h). Phases near 2π are given by dark regions and phases near zero by light regions.

Figures 13(a)–13(d) show vector plots of the supercurrent in the superconducting square for the $L=1$ state at $H_0/H_{c2}=0.27$, the $L=2$ state at $H_0/H_{c2}=0.42$, the $L=3$ state at $H_0/H_{c2}=0.67$, and the $L=4$ state at $H_0/H_{c2}=0.745$, respectively. Figures 13(e)–13(h) show the corresponding contour plots of the phase of the order parameter. Phases near 2π are given by dark regions and phases near zero by light regions. From the phase of the order parameter one can easily determine the number and the positions of the vortices. In Fig. 13(a) it is clear that the screening currents near the sample boundary flow clockwise and the currents around the

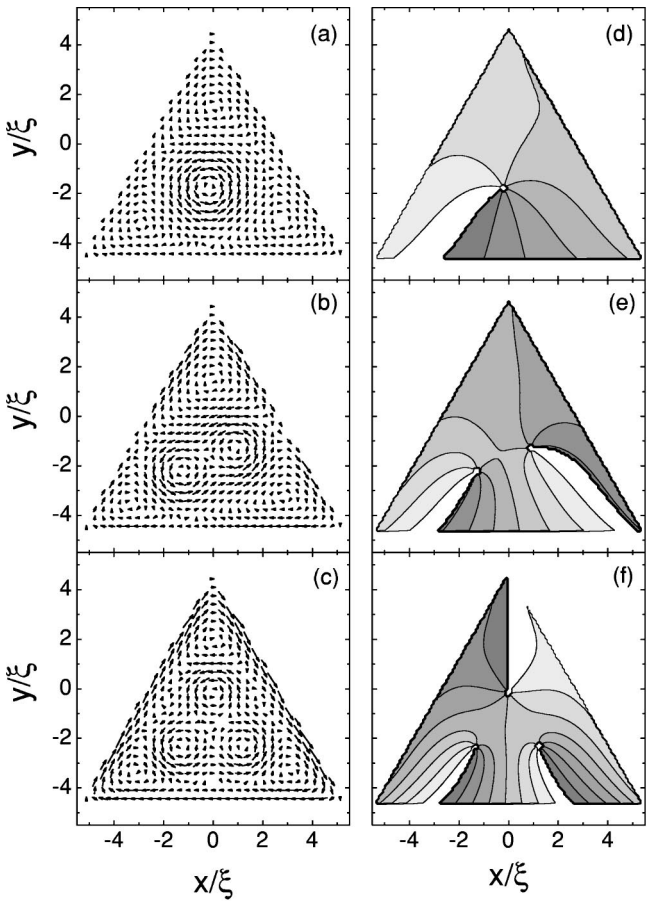

FIG. 14. (a–c) Vector plots of the supercurrent in the superconducting triangle and (d–f) contour plots of the phase of the order parameter for the $L=1$ state at $H_0/H_{c2}=0.27$ (a,d), the $L=2$ state at $H_0/H_{c2}=0.495$ (b,e), and the $L=3$ state at $H_0/H_{c2}=0.82$ (c,f). Phases near 2π are given by dark regions and phases near zero by light regions.

vortex in the center counterclockwise. In Figs. 13(b), 13(c), and 13(d) there are currents flowing counterclockwise around two, three, and four vortices, respectively. Around one vortex, the size of the current, indicated by the length of the arrows in Figs. 13(a)–13(d), is not the same for every angle. In Fig. 13(b) it is clear that in the region between the two vortices the currents around these two vortices cancel each other out. Also, in the case of $L=3$ and $L=4$ the currents around the different vortices cancel out each other in the center of the sample [see Figs. 13(c) and 13(d)].

From Figs. 13(a)–13(d) one expects antivortices towards the corners, because there are some spots where the currents flow in clockwise direction. That these are not really antivortices can be seen from the phase of the order parameter [Figs. 13(e)–13(h)]. By going around an antivortex, the phase changes with -2π and this is clearly not the case here. Moreover, the Cooper-pair density, shown in Figs. 4(a)–4(c), is not zero at these positions. In fact they are due to backflows, which are well known in hydrodynamics.

Next, we investigate the superconducting current density in the triangular sample. Figures. 14(a)–(14c) show vector plots of the supercurrent in the superconducting triangle for

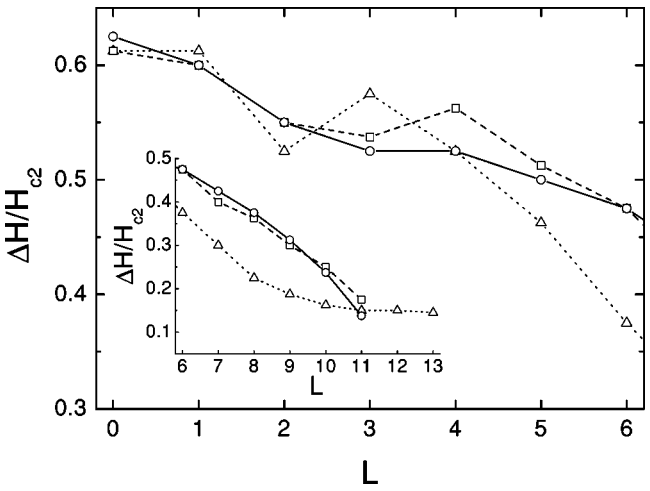

FIG. 15. The magnetic field range over which the vortex states with vorticity L are stable as a function of the vorticity L for the disk (open circles, solid curves), the square (open squares, dashed curves), and the triangle (open triangles, dotted curves).

the $L=1$ state at $H_0/H_{c2}=0.27$, the $L=2$ state at $H_0/H_{c2}=0.495$, and the $L=3$ state at $H_0/H_{c2}=0.82$, respectively. Figures 14(d)–14(f) show the contour plots of the corresponding phase of the order parameter. Phases near 2π are given by dark regions and phases near zero by light regions. The behavior of the supercurrent in triangular samples is similar to the one in square samples. The screening currents flow clockwise and the current around the vortices in the opposite direction. The currents around different vortices cancel each other in the region between them. Towards the corners, there are some spots where the current flows in a clockwise direction, but these spots are not antivortices. This can be seen from the phase of the order parameter [see Figs. 14(d)–14(f)] and from the Cooper-pair density [see Figs. 7(a) and 7(b)].

E. Stability of the vortex states

Not only the stability region of the multivortex states with respect to the giant vortex states depends on the sample geometry, but also the stability of each individual superconducting state is sensitive to the geometry. In Fig. 15 we show the magnetic field range ΔH over which the vortex state with vorticity L is stable, i.e., $\Delta H=H_{\text{expulsion}}-H_{\text{penetration}}$ [see also Figs. 16(a) and 16(b)], as a function of the vorticity L, for $L\leqslant 6$ and in the inset for $L\geqslant 6$. For the disk the result is shown by the open circles, for the square by the open squares, and for the triangle by the open triangles where the curves are guides to the eye. For the circular disk the stability region $\Delta H/H_{c2}$ uniformly decreases with increasing L with a slight dip at $L=2,3$. The square and the triangle exhibit a peak structure in the region $L<5$. For the square we find that the state with $L=4$ is stable over a larger magnetic field region than the state with vorticity $L=3$, which is a consequence of the fact that the vortex lattice tries to keep the same geometry as the sample. For the triangle we find a peak at $L=3$ and a dip at $L=2$ for the same reason. Notice that (i) the peak structure is more pronounced for structures

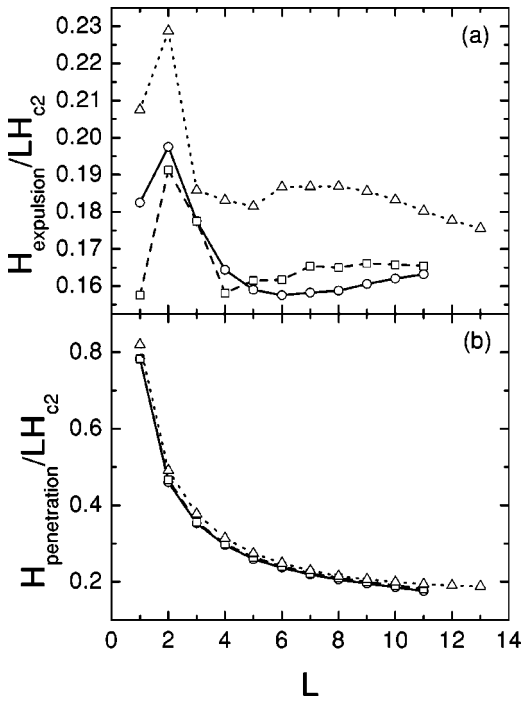

FIG. 16. (a) The expulsion field and (b) the penetration field as a function of the vorticity L for the disk (solid curves, circles), the square (dashed curves, squares), and the triangle (dotted curves, triangles).

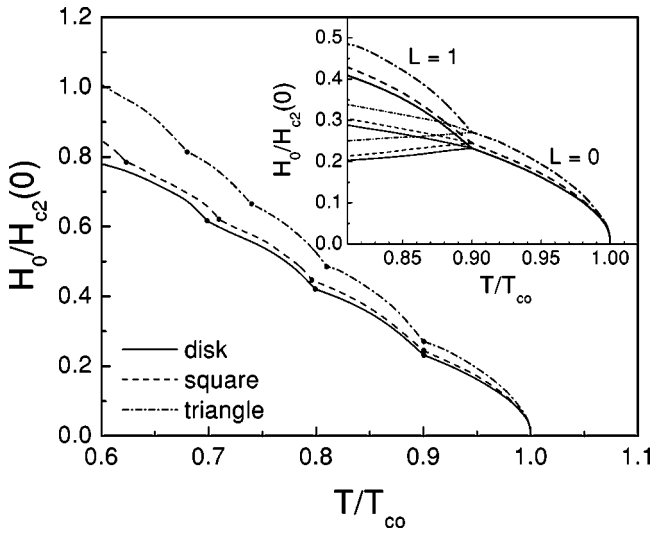

FIG. 17. The H-T phase diagram for the disk (solid curve), the square (dashed curve), and the triangle (dash-dotted curve). Only the superconducting/normal transition H_{c3} is shown as a function of temperature. The black dots indicate the transitions. The inset shows the H-T phase diagram for the states with vorticity $L=0$ and $L=1$. The thick curves are the superconducting/normal transitions and the thinner curves indicate the expulsion and the penetration.

that fit the triangular Abrikosov lattice more closely; (ii) for $L>4$ no clear peaks are found; (iii) the vortex states in the square and circle geometry have almost the same stability range for $L\leqslant 2$ and $L\geqslant 6$; (iv) for $L\geqslant 4$ the stability range for the vortex state in the triangular geometry becomes substantially smaller than that for the other two geometries that have less sharp corners. Thus sharp corners decrease the stability range of the vortex states; and (v) Fig. 2, which shows the extra flux needed to increase the vorticity by one unit, contains complementary information to Fig. 15.

F. H-T phase diagram

Until now, all our calculations were done for fixed temperature T. Now we will include temperature and our lateral dimensions and fields will be expressed in the zero-temperature results $\xi(0)$ and $H_{c2}(0)$, respectively. Temperature will be expressed in units of the zero-magnetic-field criticial temperature T_{c0}. We take the surface area of our samples $S=16\pi\xi^2(0)$ and the thickness $d=0.1\xi(0)$.

The H-T phase diagram is shown in the inset of Fig. 17 for the disk (solid curves), the square (dashed curves), and the triangle (dash-dotted curves) for the states with vorticity $L=0$ and $L=1$, thus for low fields and temperatures close to T_{c0}. The thick curves are the superconducting/normal transitions and the thinner curves indicate the expulsion and the penetration fields, i.e., the boundaries of the stability region of the state with vorticity L. The lower thin curves show the transition from the state with vorticity $L=1$ to $L=0$ with decreasing field (expulsion) and the upper thin curves show the transition from $L=0$ to $L=1$ with increasing field (penetration). Figure 17 shows the H-T phase diagram for higher fields. For the sake of clarity only the superconducting/normal transition H_{c3} is shown as a function of temperature. The black dots indicate the transition fields between the different L states. For every (fixed) temperature the superconducting/normal transition field is highest for the triangle and lowest for the disk. For every (fixed) magnetic field, the critical temperature is highest for the triangle and lowest for the disk. This means that for sharper corners, the critical temperature and critical field are enhanced due to an enhanced surface superconductivity.[15] These results are in good agreement with the phase diagrams found in Refs. 18, 23, and 24.

IV. CONCLUSIONS

We investigated theoretically the influences of the geometry of thin superconducting samples on the vortex configuration. Therefore, we considered superconducting disks, squares, and triangles with the same surface area $S=\pi 16\xi^2$ and the same thickness $d=0.1\xi$ for $\kappa=0.28$. For these three geometries we calculated the free energy and the magnetization of the different giant and multivortex states as a function of the applied magnetic field, and we indicated the multivortex to giant vortex transitions for fixed vorticity L. Multivortex states were found for disks as well as for squares and triangles for several values of the vorticity. For given L, the vortex lattice was different in the three geometries due to the fact that it tries to adapt to the geometry of the sample. This influences considerably the stability range of the different vortex states. For squares and triangles we found magnetic field regions where there is a coexistence between a giant vortex state in the center and several separated vortices in the

direction of the sample corners. Near the superconducting/normal transition we do not find multivortices, antivortices, or a combination of them, but we find surface superconductivity. Only extremely close to the superconducting/normal transition are vortex configurations containing antivortices possible. We studied the magnetic field distribution across the superconductor and around the superconductor, which clearly shows the demagnetization effects, which are very important for samples of finite thickness. The vector plots of the superconducting current showed spots where the current flows in clockwise direction. From the phase of the order parameter and the Cooper-pair density we conclude that these spots are not antivortices, but correspond to backflow currents that are typically present near sharp obstacles, i.e., corners in our case. We also investigated the stability of the vortex states with vorticity L by calculating the magnetic field range over which the vortex states with vorticity L are stable. We found that this stability range depends sensitively on the sample geometry. As a function of L we found enhanced stability for the triangle for $L=3$ and for the square for $L=4$. In the last section, we also included temperature by calculating a H-T phase diagram for the disk, the square, and the triangle. With sharper sample corners, we found that for fixed temperature, the superconducting/normal transition field H_{c3} moves to higher fields, and for fixed field, the critical temperature increases.

ACKNOWLEDGMENTS

This work was supported by the Flemish Science Foundation (FWO-Vl), the ''Onderzoeksraad van de Universiteit Antwerpen'' (GOA), the ''Interuniversity Poles of Attraction Program – Belgian State, Prime Minister's Office – Federal Office for Scientific, Technical and Cultural Affairs,'' and the European ESF–Vortex Matter. Discussions with S. Yampolskii, V. Moshchalkov, and L. Chibotaru are gratefully acknowledged.

*Electronic mail: peeters@uia.ua.ac.be

[1] O. Buisson, P. Gandit, R. Rammel, Y.Y. Wang, and B. Pannetier, Phys. Lett. A **150**, 36 (1990).
[2] A.K. Geim, I.V. Grigorieva, S.V. Dubonos, J.G.S. Lok, J.C. Maan, A.E. Filippov, and F.M. Peeters, Nature (London) **390**, 256 (1997).
[3] S. Pedersen, G.R. Kofod, J.C. Hollingbery, C.B. Sørensen, and P.E. Lindelof, Phys. Rev. B **64**, 104522 (2001).
[4] R. Benoist and W. Zwerger, Z. Phys. B: Condens. Matter **103**, 377 (1997).
[5] J.J. Palacios, Physica B **256-258**, 610 (1998); J.J. Palacios, Phys. Rev. B **58**, R5948 (1998); J.J. Palacios, Phys. Rev. Lett. **84**, 1796 (2000).
[6] V.A. Schweigert and F.M. Peeters, Phys. Rev. Lett. **83**, 2409 (1999).
[7] S.V. Yampolskii and F.M. Peeters, Phys. Rev. B **62**, 9663 (2000).
[8] E. Akkermans, D.M. Gangardt, and K. Mallick, Phys. Rev. B **62**, 12 427 (2000); E. Akkermans and K. Mallick, Physica C **332**, 250 (2000).
[9] J. Berger and J. Rubinstein, Phys. Rev. Lett. **75**, 320 (1995); J. Berger and J. Rubinstein, Phys. Rev. B **56**, 5124 (1997); **59**, 8896 (1999).
[10] V. Bruyndoncx, L. Van Look, M. Verschuere, and V.V. Moshchalkov, Phys. Rev. B **60**, 10 468 (1999).
[11] B.J. Baelus, F.M. Peeters, and V.A. Schweigert, Phys. Rev. B **63**, 144517 (2001).
[12] P.S. Deo, V.A. Schweigert, F.M. Peeters, and A.K. Geim, Phys. Rev. Lett. **79**, 4653 (1997); P.S. Deo, F.M. Peeters, and V.A. Schweigert, Superlattices Microstruct. **25**, 1195 (1999).
[13] V.A. Schweigert and F.M. Peeters, Phys. Rev. B **57**, 13 817 (1998).
[14] V.A. Schweigert, F.M. Peeters, and P.S. Deo, Phys. Rev. Lett. **81**, 2783 (1998); V.A. Schweigert and F.M. Peeters, Physica C **332**, 426 (2000).
[15] V.A. Schweigert and F.M. Peeters, Phys. Rev. B **60**, 3084 (1999).
[16] B.J. Baelus, F.M. Peeters, and V.A. Schweigert, Phys. Rev. B **61**, 9734 (2000); F.M. Peeters, V.A. Schweigert, B.J. Baelus, and P.S. Deo, Physica C **332**, 255 (2000).
[17] V.V. Moshchalkov, L. Gielen, C. Strunk, R. Jonckheere, X. Qiu, C. van Haesendonck, and Y. Bruynseraede, Nature (London) **373**, 319 (1995).
[18] V. Bruyndoncx, J.G. Rodrigo, T. Puig, L. Van Look, V.V. Moshchalkov, and R. Jonckheere, Phys. Rev. B **60**, 4285 (1999).
[19] V.M. Fomin, V.R. Misko, J.T. Devreese, and V.V. Moshchalkov, Solid State Commun. **101**, 303 (1997); V.M. Fomin, V.R. Misko, J.T. Devreese, and V.V. Moshchalkov, Phys. Rev. B **58**, 11 703 (1998).
[20] H.T. Jadallah, J. Rubinstein, and P. Sternberg, Phys. Rev. Lett. **82**, 2935 (1999).
[21] Th. Schuster, H. Kuhn, E.H. Brandt, and S. Klaumünzer, Phys. Rev. B **56**, 3413 (1997); G.P. Mikitik and E.H. Brandt, *ibid.* **62**, 6800 (2000).
[22] A. Aftalion and Q. Du, cond-mat/0101370 (unpublished).
[23] L.F. Chibotaru, A. Ceulemans, V. Bruyndoncx and V.V. Moshchalkov, Nature (London) **408**, 833 (2000).
[24] L.F. Chibotaru, A. Ceulemans, V. Bruyndoncx and V.V. Moshchalkov, Phys. Rev. Lett. **86**, 1323 (2001).
[25] J. Bonča and V.V. Kabanov, Phys. Rev. B **65**, 012509 (2002).
[26] R. Kato, Y. Enomoto, and S. Maekawa, Phys. Rev. B **47**, 8016 (1993).